General-relativistic decompression of binary neutron stars during dynamic inspiral

Mark Miller

Jet Propulsion Laboratory, California Institute of Technology, Pasadena, California 91109, USA

(Received 5 October 2005; published 2 January 2007)

We investigate the dynamic stability of inspiraling neutron stars by performing multiple-orbit numerical relativity simulations of the binary neutron star inspiral process. By introducing eccentricities in the orbits of the neutron stars, significant changes in orbital separation are obtained within orbital timescales. We find that as the binary system evolves from apastron to periastron (as the binary separation decreases), the central rest mass density of each star *decreases*, thus stabilizing the stars against individual prompt collapse. As the binary system evolves from periastron to apastron, the central rest mass density *increases*; the neutron stars recompress as the binary separation increases.

DOI: 10.1103/PhysRevD.75.024001 PACS numbers: 04.25.Dm, 04.30.Db, 04.40.Dg

I. INTRODUCTION

Detailed and accurate models of binary neutron star coalescence phenomena, from quasiequilibrium orbits through plunge and merger to the subsequent formation of the final compact object, will be required in order to extract information regarding the structure of neutron stars from detected gravitational wave signals. One detail of some debate over the past decade has been the so-called ''neutron star crushing effect'', reported in [1–3]. This effect was first reported in [1], where binary neutron star simulations employing a variety of simplifying assumptions indicated that as the binary stars spiraled inwards, the general-relativistic gravitational interaction between the two stars caused a destabilization, triggering the collapse of each star to individual black holes well *before* the plunge and merger phase of the inspiral. Since then, studies using several different sets of approximations [4–11] predict the exact opposite, namely, that the gravitational interaction between the two stars act to stabilize each star as the binary separation decreases during inspiral. An error in the formulation used in the original ''neutron star crushing effect'' studies was pointed out in [12]. However, subsequent studies still claim a destabilization effect [3].

In this Article, we report on the first fully dynamical general-relativistic simulation results aimed at studying this ''neutron star crushing effect'' for inspiraling binary neutron stars. In the past several years, fully general multiple-orbit binary neutron star simulations have been performed in numerical relativity [13,14]. We use the evolution code previously described in [13] to perform multiple-orbit simulations of binary neutron stars (for a detailed analysis of the accuracy of the simulations performed in this Article, see [15]). We begin each simulation with initial data corresponding to quasiequilibrium, circular orbit configurations modified such that the initial orbital angular velocity of the neutron stars is decreased by varying amounts. Each initial data configuration satisfies the initial value constraints of general relativity. The simulations resulting from these eccentric-orbit initial data sets permit the study, within the context of full general relativity, of the compression/decompression effect by correlating the central rest mass density of the neutron stars with the proper separation of the stars as the evolution progresses through several apastron (maximum separation)/periastron (minimum separation) points during the inspiral. We find that the stars do, in fact, stabilize as the binary separation decreases. This result is the first fully dynamic general-relativistic demonstration of the decompression of binary neutron stars; the typical simplifying assumptions made in the treatment of the problem to date, such as the truncation of a post-Newtonian expansion, the imposition of quasiequilibrium conditions, or the forcing of the spin states of the evolution of the neutron stars (e.g., forcing corotation or irrotation during the inspiral), are *not* made in the analysis presented here.

II. SIMULATION RESULTS

The numerical relativity/general-relativistic hydrodynamics code used here is described in [13] and analyzed for accuracy in [15]. The grid size used for simulations is $643 \times 643 \times 325$, employing a mirror symmetry about the equatorial plane of the neutron stars, $z = 0$. We choose units such that the gravitational constant G and the speed of light c are identically 1. A spatial discretization of $\Delta x/m = 0.148$ is used, which corresponds to roughly 40 points across the diameter of each neutron star. The boundary of the domain is thus eight neutron star diameters away from the center of mass of the system. The physical parameters of three simulations NS-1, NS-2, and NS-3 are shown in Table I. The initial data corresponds to the quasiequilibrium, corotating, circular orbit initial data described in [13], except that here, the initial orbital angular velocity parameter Ω_0 has been decreased from the circular orbit value by a factor of 1%, 2%, and 3% for simulation NS-1, NS-2, and NS-3, respectively. The resulting initial data satisfies the Einstein equation initial value constraints, and results in binary evolutions whose orbits contain increasing amounts of eccentricity.

The initial spin state of each of the neutron stars corresponds to a corotation with the initial orbital angular

TABLE I. The physical parameters of the initial data used for numerical relativity simulations NS-1, NS-2, and NS-3. These initial data sets correspond to quasiequilibrium, corotating, circular orbit initial data with the initial angular velocity Ω_0 reduced from the circular orbit value by 1%, 2%, and 3%, respectively. The symbols J_0 and M_0 are used to denote the initial angular momentum and total rest mass of the configuration, respectively. The initial proper separation of the neutron stars, defined by Eq. 57 in [13], is denoted as $(r_p)_0$. A polytropic equation of state with adiabatic index $\Gamma = 2$ is used. The rest mass of each neutron star corresponds to 82% of the maximum stable TOV rest mass configuration. All physical quantities in this Article are expressed in units of m, which we define to be twice the ADM mass of a single stationary neutron star configuration with rest mass $M_0/2$ uniformly rotating with angular velocity Ω_0.

Config.	$m\Omega_0$	J_0/m^2	M_0/m	$(r_p)_0/m$
NS-1	0.01618	1.121	1.073	18.10
NS-2	0.01599	1.094	1.073	18.12
NS-3	0.01580	1.067	1.073	18.14

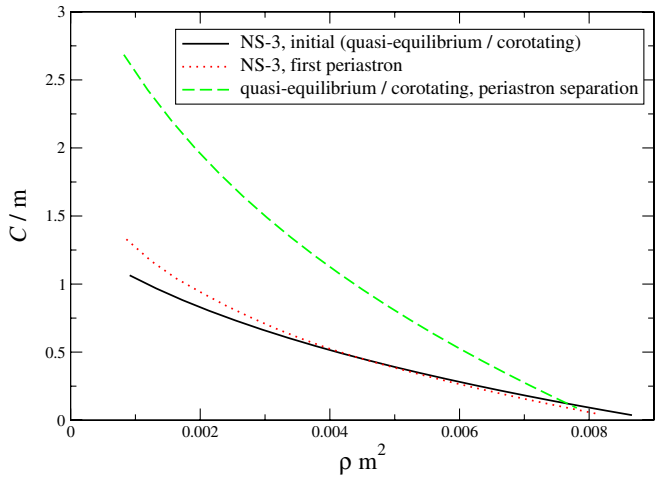

FIG. 1 (color online). The circulation $C = \oint_{\mathcal{C}_\rho} d\sigma\, h u_\mu (\frac{\partial}{\partial\sigma})^\mu$ (h is the relativistic specific enthalpy of the neutron star fluid, u^μ is the 4-velocity of the neutron star fluid, and σ is a Lagrange parameter labeling points on the curve) along constant rest mass density curves $\mathcal{C}_\rho$ in the equatorial plane of the neutron stars is plotted as a function of rest mass density for three different neutron star binary configurations. The first (solid) curve shows the circulation of the initial corotating, quasiequilibrium binary configuration of simulation NS-3, while the second (dotted) curve shows the circulation of the binary configuration of simulation NS-3 at the time corresponding to the first periastron point. For comparison, the circulation of a corotating, quasiequilibrium, equivalent rest mass binary configuration with a proper separation equal to that of simulation NS-3 at periastron is plotted (dashed curve). Clearly, the spin of the neutron stars during the numerical evolution NS-3 remains roughly constant. This is in stark contrast to a corotating quasiequilibrium sequence in which the neutron stars are artificially "spun-up" as the binary separation decreases.

velocity. For binary neutron stars of 1.4 solar masses each, this corresponds to a spin period of approximately 5 milliseconds. However, it is important to note that during the dynamical evolution, the spins of the neutron stars do not remain tidally locked to the orbital angular velocity (see Fig. 1). Previous quasiequilibrium sequence inspiral studies have assumed either strictly corotating or strictly irrotational neutron star spin scenarios; in these cases, the spin states of the neutron stars are fixed to have either corotating spin or to be irrotational during the inspiral sequence. By numerically solving the general coupled Einstein/hydrodynamics equations, we are able to study the more astrophysically relevant case where the nonzero spin of each neutron star actually evolves in time via the equations of motion.

In Fig. 2, the angular momentum of the binary system simulations is plotted as a function of coordinate time; $t_{\rm coord} = 500$ m corresponds to roughly two orbital periods. For comparison, the angular momentum for solutions to the 2.5 post-Newtonian (dotted curves) and 4.5 post-Newtonian (dashed curves) point particle equations of motion is plotted along side the simulation results (solid curves). The overall rate of decrease in angular momentum for the numerical relativity simulations is roughly equivalent, if not slightly more, than predicted by the post-Newtonian equations of motion. However, the difference in total angular momentum between the numerical relativity simulations NS-1, NS-2, and NS-3 (solid curves) is

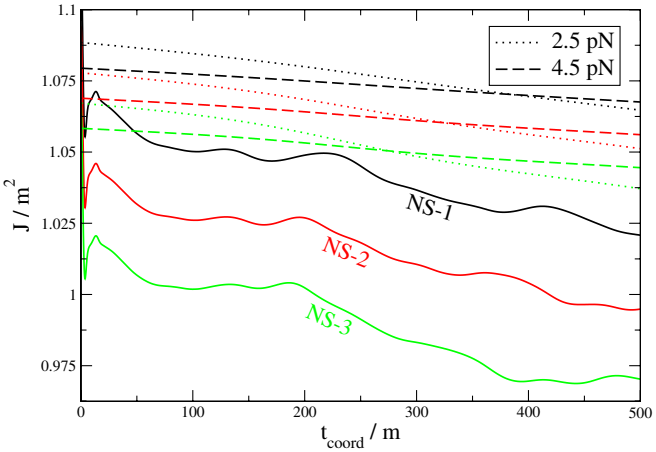

FIG. 2 (color online). The total angular momentum J is plotted for the binary neutron star numerical relativity simulations NS-1, NS-2, and NS-3 (solid curves). All simulations correspond to roughly two orbital periods. For comparison, solutions to the post-Newtonian point particle equations of motion are shown, using the same initial coordinate separation, mass, and initial orbital angular velocity (i.e., 1%, 2%, and 3% below the circular orbit angular velocity) as the numerical relativity simulations. Dotted curves are solutions to the 2.5 post-Newtonian (quadrupole level) equations of motion (see, e.g., [16]). Dashed curves are solutions to the 4.5 post-Newtonian equations of motion, which include 3.5 pN [16] and 4.5 pN [17] radiation reaction terms, along with the 3.0 pN [18] conservative terms.

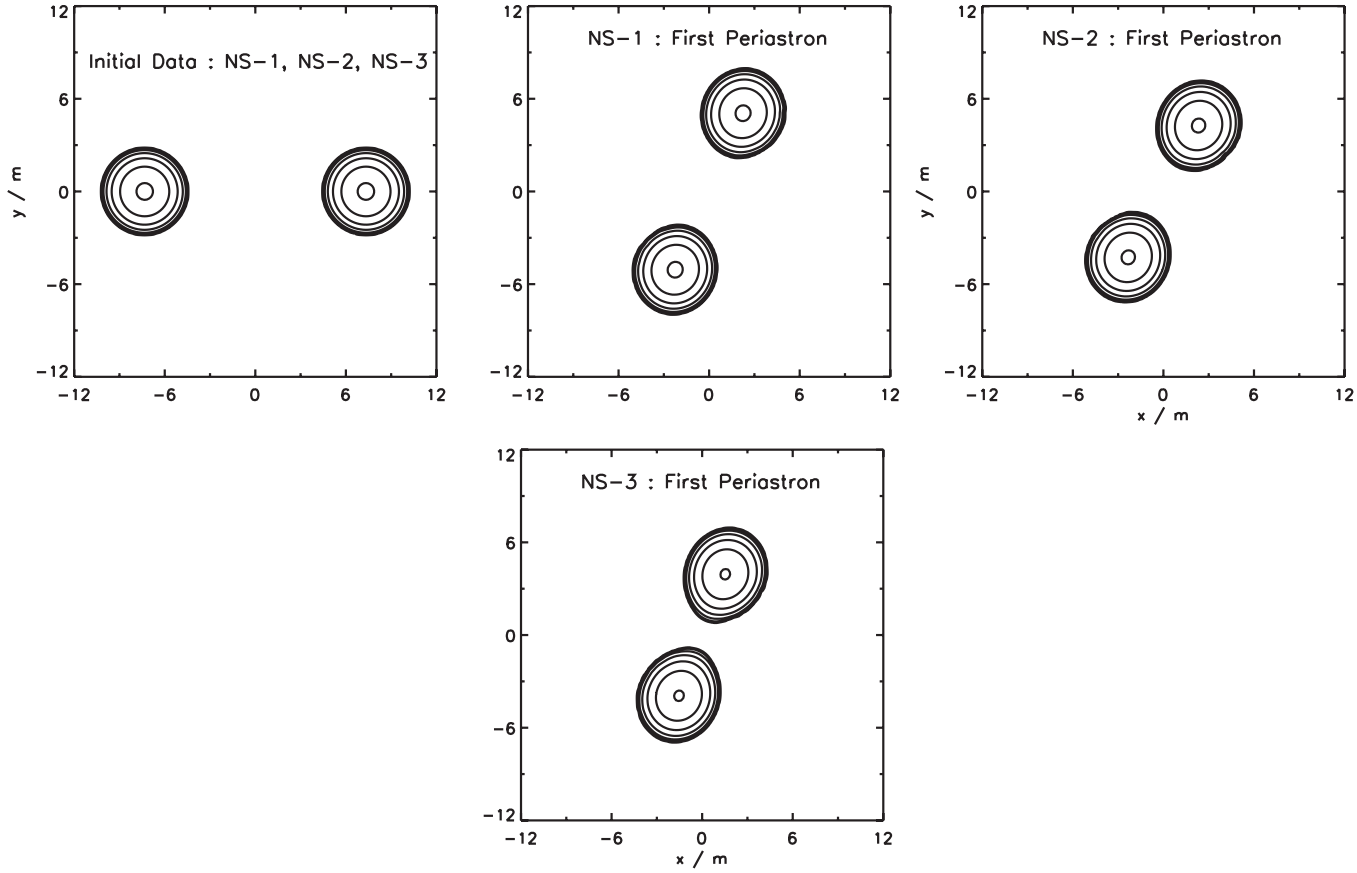

FIG. 3. Contour plots of the rest mass density ρ in the $x-y$ equatorial plane of the binary neutron stars is shown for initial data (upper left) and the first periastron point for simulations NS-1 (upper right), NS-2 (lower left), and NS-3 (lower right). The central contour corresponds to a value of $\rho = 0.0083/m^2$. Six more contours are shown; each successive contour corresponds to a decrease in rest mass density by a factor of 2.

nearly twice as large as the difference between the post-Newtonian curves, even though the post-Newtonian initial data is selected using the same method as in the numerical relativity case, namely, using circular orbit initial data with a decrease in initial angular velocity of 1%, 2%, and 3% (see Table I). This is most likely due to the nonlinear effects of resolving the constraints of general relativity after decreasing the initial angular velocity parameter Ω_0 when preparing the initial data for the numerical relativity simulations.

Contour plots of the rest mass density for the initial data, as well as the first periastron points of simulations NS-1, NS-2, and NS-3, are shown in Fig. 3. The first periastron points occur just slightly before the completion of three-quarters of an orbit for all three simulations.

III. DECOMPRESSION OF BINARY NEUTRON STARS

In Fig. 4, we plot the proper binary separation r_p (defined to be the spatial geodesic distance between the maximum rest mass density point of each neutron star, see Eq. 57 in [13]) as a function of the proper time t_p measured by observers located at the maximum rest mass density points of the neutron stars. An evolved proper time of $t_p = 300$ m corresponds to roughly two orbital periods. Also in Fig. 4 is a plot of the maximum rest mass density $\rho_{\max}$ of the neutron stars as a function of proper time t_p. Oscillations in $\rho_{\max}(t_p)$ corresponding to the fundamental radial oscillation mode of each neutron star have been filtered out (these oscillations have a proper period of $T_p = 35.0$ m). Figure 4 displays a clear correlation between the maximum rest mass density of the stars and the proper separation of the stars; smaller proper separation r_p corresponds to smaller maximum rest mass density $\rho_{\max}$. More quantitatively, the correlation $\mathrm{Cor}(r_p, \rho_{\max})$ between the proper binary separation and the maximum rest mass density is computed to be

$$\mathrm{Cor}\,(r_p, \rho_{\max}) > 0.95 \qquad (1)$$

for all simulations. Convergence tests on simulation NS-3 yields a Richardson extrapolation value of $\mathrm{Cor}(r_p, \rho_{\max}) = 1.00$ (see Fig. 5).

Figure 4 also shows that the correlation between orbital separation and maximum rest mass density exists over gravitational radiation reaction timescales. This is evi-

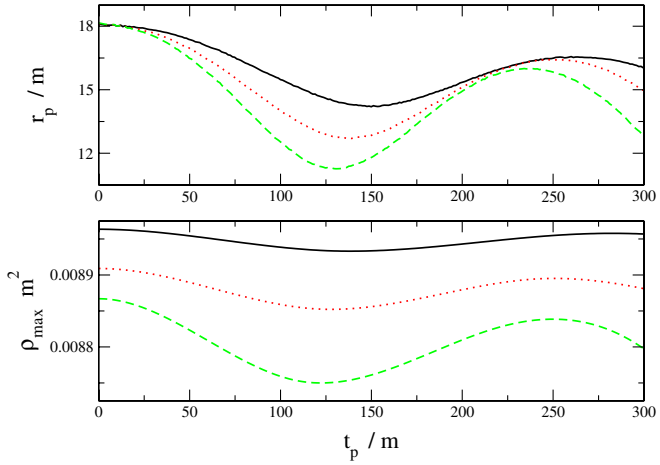

FIG. 4 (color online). Top panel: the proper separation of the binary r_p is plotted as a function of proper time t_p as measured by observers at the maximum rest mass density $\rho_{\max}$ of the neutron stars, for numerical relativity simulations NS-1 (solid curve), NS-2 (dotted curve), and NS-3 (dashed curve). Bottom panel: the maximum rest mass density $\rho_{\max}$ of the neutron stars is plotted as a function of t_p for numerical relativity simulations NS-1 (solid curve), NS-2 (dotted curve), and NS-3 (dashed curve). Oscillations in $\rho_{\max}(t_p)$ corresponding to the fundamental radial oscillation mode of each neutron star have been filtered out.

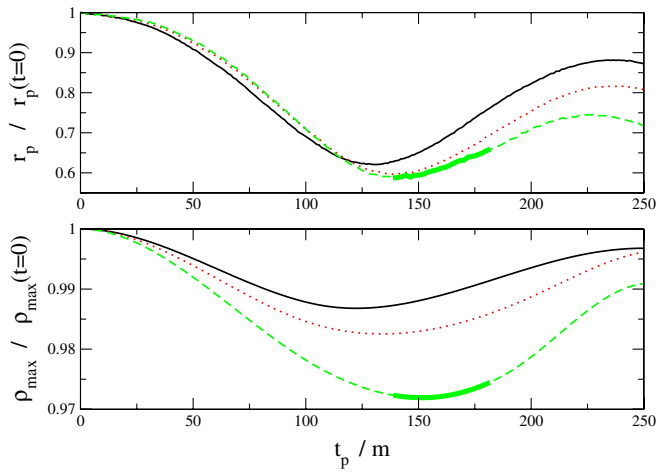

FIG. 5 (color online). The proper separation of the binary (top panel) and maximum rest mass density (bottom panel) are plotted as a function of proper time; each quantity is normalized by its initial value. Shown are NS-3 simulation results (solid curve). The simulation was repeated for different resolutions and grid sizes: the dotted curves are results obtained using $323 \times 323 \times 165$ grid points with $\Delta x/m = 0.211$; the dashed curves are results obtained using $195 \times 195 \times 101$ grid points with $\Delta x/m = 0.247$ (the thick, solid sections of these low-resolution curves represent when the neutron stars are in contact with each other). The Richardson extrapolation of the correlation $\mathrm{Cor}(r_p, \rho_{\max})$ between the proper binary separation and the maximum rest mass density is 1.00.

denced by comparing both the proper separation of the binary and the maximum rest mass density at successive apastron (local maximum in separation) points in Fig. 4. First, we see that the proper separation r_p at the second apastron point (which occurs at roughly $t_p = 250$ m for all three simulations) is approximately 10% smaller than the proper separation at the first apastron point (which occurs at the initial time $t_p = 0$). Gravitational radiation emission drains the binding energy of the binary, causing an overall decrease in separation from one apastron point to the next. We also see from Fig. 4 that the maximum rest mass density of the neutron stars is smaller at the second apastron point as compared to the first apastron point. Thus, these simulations also demonstrate the correlation between orbital separation and maximum rest mass density on gravitational radiation reaction timescales.

In [8], a post-Newtonian matched asymptotic expansion technique is used to obtain an expression for the fractional change in the central density ρ_c of inspiraling binary neutron stars, perturbative in powers of the "tidal expansion parameter" $\alpha \equiv R/r$ where R is the stellar radius and r is the binary separation, such that

$$\frac{\delta\rho_c}{\rho_c} \propto \alpha^6 \tag{2}$$

as $\alpha \to 0$. That is, when the fractional change in the central rest mass density of the stars is expanded about $\alpha = 0$ (i.e. infinite binary separation) in powers of α, post-Newtonian theory predicts the first nonzero term to be α^6. We note that the limited range of binary separations, along with the large values of α obtained in our simulations ($\alpha = R_p/r_p \approx 0.4$, where R_p is the proper stellar radius computed from the proper stellar volume V_p according to $R_p = (3V_p/(4\pi))^{1/3}$), prevent us from accurately determining the power of the first nonzero term in an expansion of the fractional change in the central rest mass density as in, e.g., Eq. (2). Simulations involving much smaller values of α (larger binary separations, which imply longer orbital periods), which will only be capable with adaptive mesh refinement technology and/or higher order methods, will be required to verify the post-Newtonian prediction Eq. (2).

ACKNOWLEDGMENTS

It is a pleasure to thank my colleagues at the Jet Propulsion Laboratory for many useful discussions and suggestions. Financial support for this research has been provided by the Jet Propulsion Laboratory under contract with the National Aeronautics and Space Administration. Computational resource support has been provided by the JPL Institutional Computing and Information Services, the NASA Directorates of Aeronautics Research, Science, Exploration Systems, and Space Operations, and NSF NRAC project No. MCA02N022.

[1] J. Wilson and G. Mathews, Phys. Rev. Lett. **75**, 4161 (1995).
[2] J. Wilson, G. Mathews, and P. Marronetti, Phys. Rev. D **54**, 1317 (1996); G. Mathews and J. Wilson, Astrophys. J. **482**, 929 (1997); P. Marronetti, G. Mathews, and J. R. Wilson, Phys. Rev. D **58**, 107503 (1998); G. Mathews, P. Marronetti, and J. Wilson, Phys. Rev. D **58**, 043003 (1998).
[3] G. Mathews and J. Wilson, Phys. Rev. D **61**, 127304 (2000); J. Wilson, Phys. Rev. D **66**, 084015 (2002); J. Wilson and G. Mathews, Astrophys. J. **610**, 368 (2004); D. S. P. Dearborn, J. Wilson, and G. Mathews, Astrophys. J. **630**, 309 (2005).
[4] D. Lai, Phys. Rev. Lett. **76**, 4878 (1996).
[5] A. G. Wiseman, Phys. Rev. Lett. **79**, 1189 (1997).
[6] P. R. Brady and S. A. Hughes, Phys. Rev. Lett. **79**, 1186 (1997).
[7] T. W. Baumgarte, G. B. Cook, M. A. Scheel, S. L. Shapiro, and S. A. Teukolsky, Phys. Rev. Lett. **79**, 1182 (1997).
[8] E. E. Flanagan, Phys. Rev. D **58**, 124030 (1998).
[9] K. S. Thorne, Phys. Rev. D **58**, 124031 (1998).
[10] E. Gourgoulhon, P. Grandclément, K. Taniguchi, J. Marck, and S. Bonazzola, Phys. Rev. D **63**, 064029 (2001).
[11] K. Taniguchi and E. Gourgoulhon, Phys. Rev. D **68**, 124025 (2003).
[12] E. Flannagan, Phys. Rev. Lett. **82**, 1354 (1999).
[13] M. Miller, P. Gressman, and W.-M. Suen, Phys. Rev. D **69**, 064026 (2004).
[14] P. Marronetti, M. D. Duez, S. L. Shapiro, and T. W. Baumgarte, Phys. Rev. Lett. **92**, 141101 (2004).
[15] M. Miller, Phys. Rev. D **71**, 104016 (2005).
[16] M. E. Pati and C. M. Will, Phys. Rev. D **65**, 104008 (2002).
[17] A. Gopakumar, B. Iyer, and S. Iyer, Phys. Rev. D **55**, 6030 (1997).
[18] L. Blanchet and B. Iyer, Class. Quant. Grav. **20**, 755 (2003).